X-ray excited luminescence and local structures in Tb-doped Y_2O_3 nanocrystals

Y. L. Soo, S. W. Huang, Z. H. Ming, and Y. H. Kao
Department of Physics, State University of New York at Buffalo, Amherst, New York 14260

G. C. Smith
Brookhaven National Laboratory, Upton, New York 11973

E. Goldburt, R. Hodel, B. Kulkarni, J. V. D. Veliadis, and R. N. Bhargava
Nanocrystals Technology, P.O. Box 820, Briarcliff Manor, New York 10510

(Received 8 August 1997; accepted for publication 3 February 1998)

Pronounced structure in x-ray excited luminescence (XEL) has been observed in dilute Tb-doped Y_2O_3 (Y_2O_3:Tb) nanocrystals. This effect affords a means to assess different energy transfer mechanisms in the nanocrystals and also an opportunity for novel device applications. Sharp jumps and oscillations are found in the XEL output with the incident x-ray energy around the absorption edges of Y and Tb. When compared with a bulk Y_2O_3:Tb sample, these effects are attributed to some unique electronic and optical properties of doped nanocrystals related to quantum confinement of charge carriers, and the main features can be explained by a proposed model of multichannel energy transfer. Extended x-ray absorption fine structure techniques have also been employed to study the effect of size variation and chemical doping on the local structures in Y_2O_3 and Y_2O_3:Tb nanocrystals. The local environment surrounding Y and Tb in the nanocrystals is compared with that in the respective bulk material. The results indicate that Tb impurity atoms substitute for Y sites in bulk Y_2O_3, while doping in the nanocrystals is complicated by the large fraction of surface atoms and local disorder. © *1998 American Institute of Physics.* [S0021-8979(98)00610-0]

I. INTRODUCTION

Small crystalline particles exhibit many novel physical properties not found in bulk materials. These nanocrystals (quantum dots) are of considerable interest for both technological applications and fundamental studies. Of particular interest are the doped nanocrystals (henceforth referred to as DNC), as demonstrated by Bhargava *et al.* that Mn-doped ZnS nanocrystals show high efficiency of photoluminescence (PL) and ultrafast electron-hole recombination rates.[1,2] More recently, an increase in PL efficiency with reduced particle size in Tb-doped Y_2O_3 nanocrystal phosphors[3,4] has also been reported. Novel physical behavior can be expected in these systems as the particle size is reduced to become comparable with some characteristic lengths such as the electronic de Broglie wavelength, the effective Bohr radius around the impurity centers, or the exciton radius. In addition to these commonly known quantum size effects, however, the excited states of the localized atoms (e.g., Tb in Y_2O_3) can be strongly modulated as a result of quantum confinement in the nanoparticles (referred to as quantum confined atoms), which can lead to changes in the overlap of wave functions with other atoms in the quantum dots. Due to this modulation effect of quantum confinement,[5–7] the impurity states in a DNC can interact more efficiently with the host than in the bulk, leading to significant changes in the electronic energy structure and transition probabilities.

In contrast to ZnS:Mn nanocrystals which emit yellow photoluminescence, phosphors of Tb-doped nanocrystals of Y_2O_3 with size distribution ranging from 30 to 50 Å can down-convert absorbed x-ray or ultraviolet photons to green luminescence. During the course of the present experiment, we have found element-specific absorption-edge features in the x-ray excited luminescence (XEL) spectrum, showing ''edge jumps'' when the incident x-ray energy is at the absorption edges of either the activators (Tb) or Y atoms in the host. These observations allow us to compare the efficiency of different down-conversion paths in various samples with different particle sizes. The results also provide useful insights into the underlying mechanisms responsible for some novel optical and electronic properties.

It is believed that these intriguing optical and electronic properties of DNC are closely related to the local environment surrounding the impurity atoms. In order to explore the novel properties of DNC phosphors for device applications, a physical understanding of the local structural changes from bulk to nanoparticles is an important prerequisite. Since the small host particle and the dopants do not have long-range order, conventional x-ray diffraction techniques are not useful for structural investigation. To this end, extended x-ray absorption fine structure (EXAFS) spectroscopy, a tool for short-range order studies, is well suited for this task. In the present work, EXAFS technique is employed to investigate the local structures around Tb and Y atoms in both undoped and Tb-doped Y_2O_3 nanocrystal phosphors. In addition, bulk Y_2O_3 and Y_2O_3:Tb materials are also studied for comparison.

II. EXPERIMENT

Sol-gel processing techniques were used to synthesize Y_2O_3:Tb nanocrystals.[3,4,8] First, metallic sodium was reacted

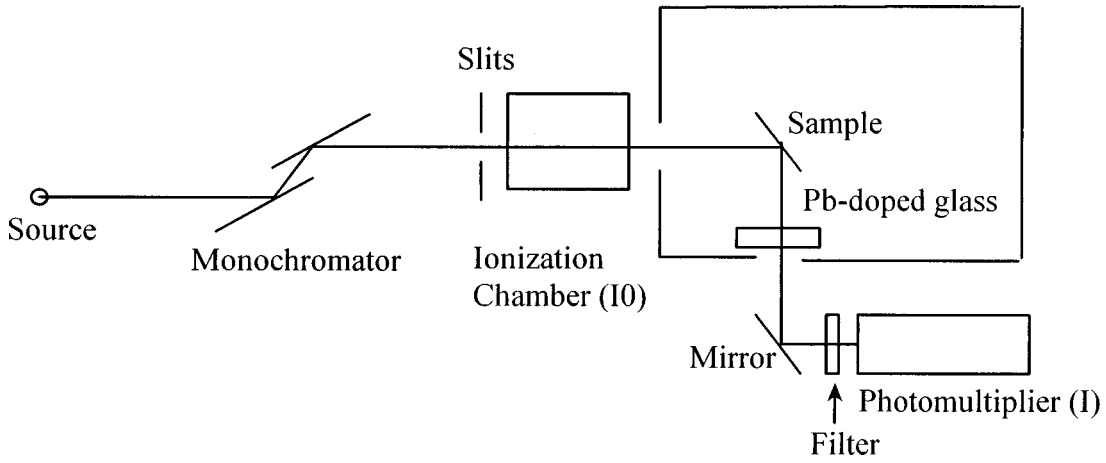

FIG. 1. Experimental setup for x-ray excited luminescence (XEL) experiments.

with iso-propanol quantitatively resulting in sodium iso-propoxide. The latter was reacted with yttrium and terbium chlorides to obtain yttrium and terbium iso-propoxides. Yttrium and terbium iso-propoxides were combined in azeotropic distillation of butanol to exchange the iso-propoxide to butoxide groups. A fivefold excess of *n*-butanol was used. The resulting yttrium *n*-butoxide was used as a stock solution and was combined with yttrium butoxide which was prepared separately to vary the Tb-dopant concentration in the nanocrystals. Tb-doped Y_2O_3 nanocrystals were prepared with various ratios of yttrium and yttrium-dopant precursors.

The size distribution of the DNC particles ranges from 25 to 55 Å as determined by transmission electron microscopy (TEM). All these samples showed relatively high PL efficiency in the green, attributed to $^5D_4-^7F_5$ transition of Tb^{3+} ion. The Tb content in the nanocrystals was found to be 1–5 at % using energy dispersive x-ray spectroscopy. The XEL and EXAFS experiments were performed at beamline X3B1 of National Synchrotron Light Source at Brookhaven National Laboratory using a custom-built visible photon collection setup (Fig. 1) and a conventional fluorescence mode of detection, respectively. All measurements were made at room temperature.

The intensity of XEL output was measured as a function of incident x-ray energy near the Tb *L* edges and Y *K* edge for a series of Y_2O_3:Tb DNC phosphors (samples A–C, processed under slightly different conditions) as well as a bulk Y_2O_3:Tb sample. All these samples were thin films deposited on glass slides. As shown in Fig. 1, a piece of Pb-doped glass transparent to visible light but opaque to x rays was employed to reject the scattered and fluorescent x rays from the sample. A mirror was used to reflect the visible light at 90° into a photomultiplier. This mirror also served the purpose of eliminating possible residual x rays passing through the upstream Pb-doped glass. A filter was placed in front of the photomultiplier to reject possible blue to ultraviolet photons. The XEL spectra near the Tb *L* edges and the Y *K* edge are normalized to the prejump intensities at 7.5 and 17 keV as shown in Figs. 2 and 3, respectively.

We have investigated the local structures around Y and Tb atoms in Y_2O_3:Tb DNC phosphors using fluorescence EXAFS at the Y *K* edge and Tb L_1 edge, respectively. For the need of model compounds and also for the sake of comparison, EXAFS spectra of bulk Y_2O_3 and bulk Y_2O_3:Tb samples were also obtained in the same experiment. To study the effect of Tb doping and that of decreased particle size of the Y_2O_3 host, we have made a comparison of the Y *K* edge EXAFS of a DNC Y_2O_3:Tb sample with a bulk Y_2O_3:Tb and with an undoped nanocrystal Y_2O_3. A well-established background subtraction and correction method was used to extract the EXAFS χ functions from the raw experimental data.[9,10] The χ functions were then weighted with k^3 and Fourier transformed into real space for detailed comparison.[11,12] For a quantitative analysis of the local structures, the experimental data were analyzed and compared

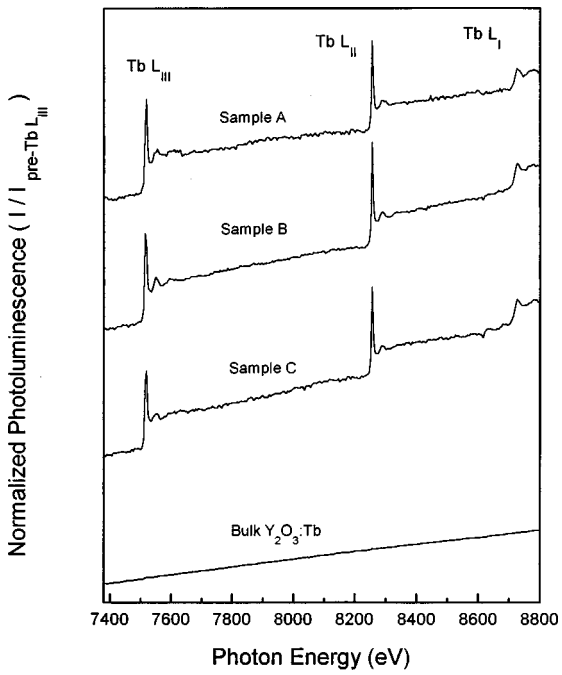

FIG. 2. X-ray excited luminescence near Tb *L* edges. Curves have been shifted vertically for the sake of clarity.

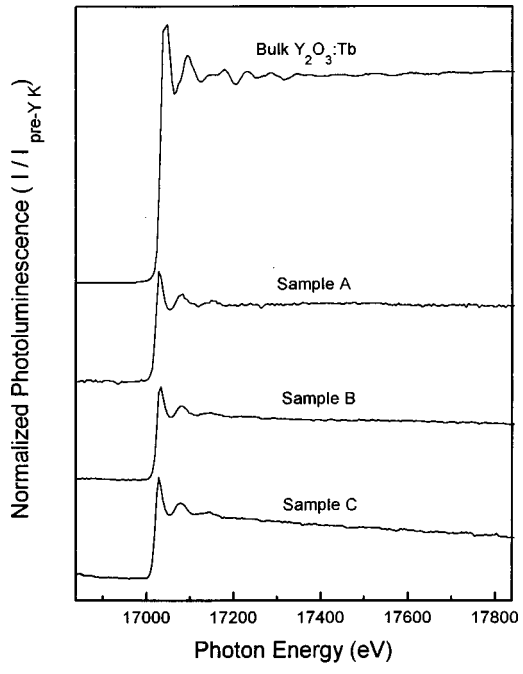

FIG. 3. X-ray excited luminescence near Y *K* edge. Curves have been shifted vertically for the sake of clarity.

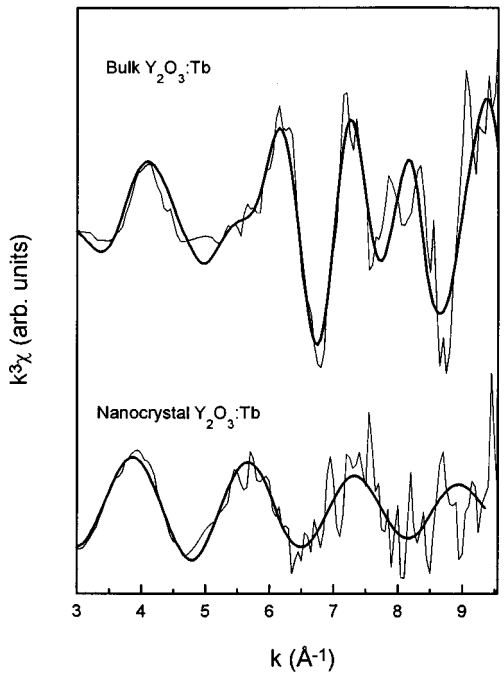

FIG. 5. Weighted Tb L_1 edge EXAFS χ functions. Fine line: experimental; coarse line: theoretical.

with theoretical calculations by an improved curve fitting method.[9,11–13] The EXAFS χ functions and theoretical curves obtained from curve fitting are shown in Figs. 4 and 5 and the corresponding Fourier transforms are shown in Figs. 6 and 7 for Y-*K* and Tb-L_1 EXAFS, respectively. The parameters obtained from this fitting process are listed in Table I for the local structures around the Y atoms and in Table II for the local structures around the Tb atoms.

III. RESULTS AND DISCUSSION

An interesting outcome of the x-ray absorption experiments is the observation of pronounced green XEL output when the DNC is excited by incident x rays with energy at the absorption edges of Tb and Y. These measurements were made by using the setup illustrated in Fig. 1 and the results are shown in Figs. 2 and 3. The 542 nm green light output, characteristic of transitions from $4f^8$ manifolds of Tb^{3+},

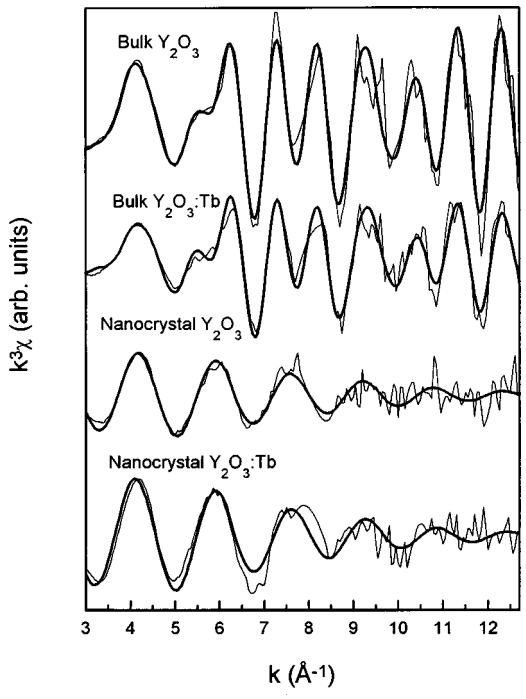

FIG. 4. Weighted Y *K* edge EXAFS χ functions. Fine line: experimental; coarse line: theoretical.

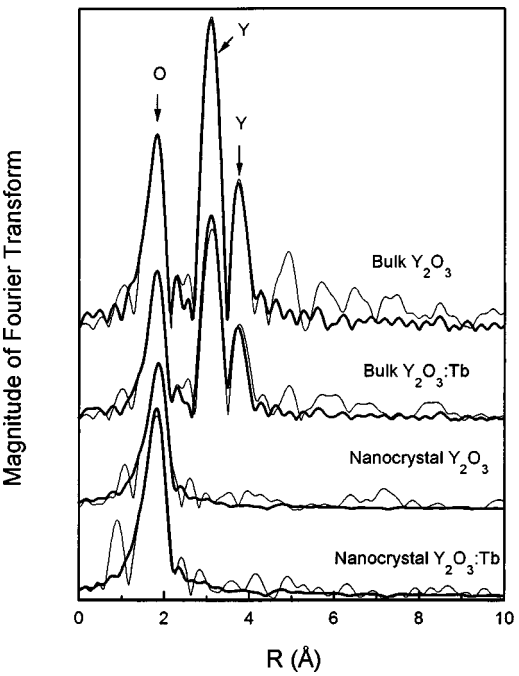

FIG. 6. Fourier transform of Y *K* edge EXAFS χ functions. Fine line: experimental; coarse line: theoretical.

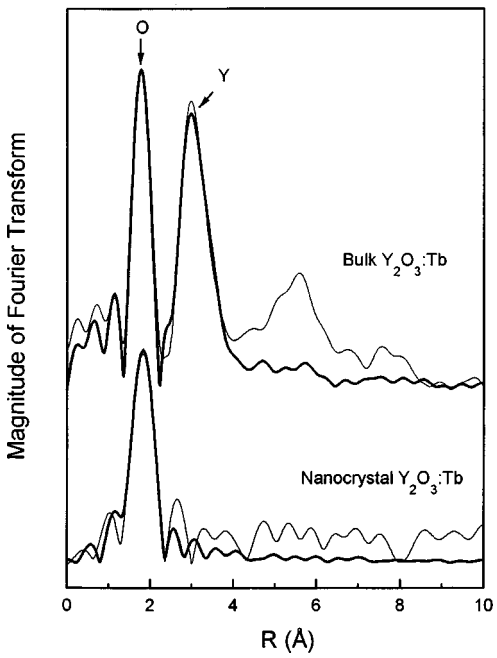

FIG. 7. Fourier transform of Tb L_1 edge EXAFS χ functions. Fine line: experimental; coarse line: theoretical.

shows sharp ''XEL edge jumps'' as well as EXAFS oscillations similar to those found in the usual x-ray fluorescence. However, a significant difference in the XEL output was found between the nanocrystals and bulk material. This is illustrated in Fig. 8. The conversion of x-ray excitation to visible XEL could involve two distinct paths: (i) direct absorption of incident photons by the activator (dopant) atom which gives rise directly to the Tb-activator edge jumps, and (ii) absorption of incident photons by the host material atom (Y) followed by an energy transfer to the activator which causes the host (Y) edge jump. Following the x-ray excitation, the absorbed energy ($h\nu$) may subsequently be emitted via the usual x-ray fluorescence process (denoted by $h\nu'$ and $h\nu''$ for photons originated from the host or the activator, respectively), and it may also be down-converted to create photoexcited charge carriers in the band states (via the dotted-line path), thereby giving rise to the observed visible light output (dash-dotted line path) through electron-hole recombination.

Although x-ray fluorescence can propagate through a distance larger than the size of the nanoparticles, the photoexcited carriers are nevertheless confined within the small particle boundaries. Due to this effect of quantum confinement, it is expected that energy transfer via excited carriers in DNC will depend on particle size and is rather different from that in the corresponding bulk material. This is consistent with the observation that PL efficiency in Y_2O_3:Tb increases with decreasing particle sizes. The width of the $4f^75d$ absorption band has been observed as a function of the nanoparticle size. The broadened absorption band and subsequent transfer of charges to the $4f^8$ state are believed to be responsible for the enhanced PL efficiency. The size of nanoparticles was measured using TEM. The efficiency was found to vary as $1/D^2$, where D is the mean diameter of

TABLE I. Local structures around Y for samples obtained from Y K EXAFS curve fitting. Underlined values were kept constant during fitting. Coordination number (N) and interatomic distances (R) of bulk Y_2O_3 are calculated from x-ray diffraction data edited by Wyckoff (see Ref. 16), and σ^2 is a Debye–Waller factor serving as a measure of the local disorder.

Sample	Atom	N	R (Å)	σ^2 (10^{-3} Å^2)	ΔE_0 (eV)	λ (Å)	S_0^2
Bulk Y_2O_3.	O	4.5	2.27	4	−0.2	5	0.8
	O	1.5	2.33	10	−2		
	Y	6	3.51	4	−5		
	O	1.5	3.97	48	2		
	Y	6	4.02	6	2		
Bulk Y_2O_3 :Tb	O	4.1	2.27	4	1	5	0.8
	O	1.5	2.33	12	−18		
	Y	6	3.51	6	−4		
	O	1.5	3.97	136	−10		
	Y	6	4.02	9	1		
Nanocrystal Y_2O_3.	O	5.7	2.33	9	5	5	0.8
Nanocrystal Y_2O_3 :Tb	O	7.8	2.31	10	2	5	0.8

nanoparticles.[14] This result is also similar to that found in the ZnS:Mn system.[15]

The ratio of the ''XEL edge jump'' signal to the monotonic increasing background signal is about 70 times higher in the DNC samples than that in the bulk materials, as shown in Fig. 2. This enhanced ratio in DNC can be attributed to a reduced background signal. The severe reduction of the background signal in DNC is due to enhanced nonradiative contribution of the surface. The smallness of the size of DNC hinders the energy transfer from the x-ray absorbing atoms in the host to the activator Tb atoms (via the ''host'' path illustrated in Fig. 8). Such a background reduction is particularly significant for the Tb-activator atoms residing near the surface of nanoparticles. This is also consistent with our K edge results of Y shown in Fig. 3 where the ratio of ''edge jump'' to the background in the bulk sample at the K edge of Y is about three times higher than that in the DNC samples despite the presence of far-reaching Y $K\alpha$ fluorescence. These observations therefore allow us to assess the relatively different contributions to the XEL output arising from the different x-ray energy down-conversion paths.

The local structures around Y and Tb atoms have been studied by EXAFS. The Fourier transforms of the Y K edge EXAFS χ functions for four different samples are shown in Fig. 6. The first peak is due to the nearest-neighbor oxygen atoms. For the bulk Y_2O_3 and Y_2O_3:Tb samples, the second and third peaks arise from other Y atoms located at distances of 3.51 and 4.02 Å from the central x-ray absorbing Y atoms, respectively. In view of the close curve fitting agreement of

TABLE II. Local structures around Tb for each sample obtained from Tb-L_I EXAFS curve fitting. Underlined values were kept constant during fitting.

Sample	Atom	N	R (Å)	σ^2 (10^{-3} Å^2)	ΔE_0 (eV)	λ (Å)	S_0^2
Bulk Y_2O_3 :Tb	O	6	2.37	0.2	−1	10	0.63
	Y	6	3.51	0.3	−15		
	Y	6	4.09	2	−2		
Nanocrystal Y_2O_3 :Tb	O	8.4	2.42	7	−5		0.63

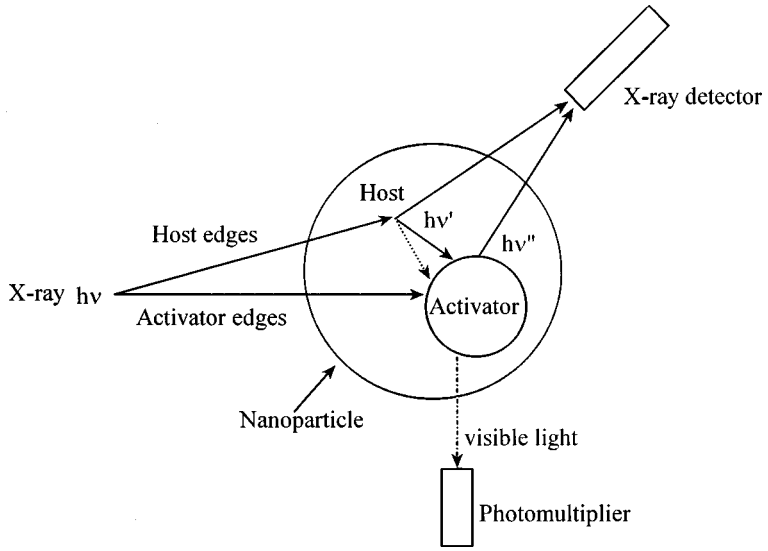

FIG. 8. Schematic illustration of the proposed energy transfer model for x-ray excited luminescence from DNC phosphors.

the EXAFS data with theoretical calculations, these results are consistent with the known structure of bulk Y_2O_3. The presence of Y-neighbor peaks in bulk Y_2O_3:Tb at interatomic distances similar to those in bulk Y_2O_3 indicates that doping the bulk Y_2O_3 host with a small amount of Tb does not change the local environment surrounding the Y atoms, as expected. Other peaks at distances larger than 4.5 Å are mainly caused by Fourier transform processing, therefore they are not reliable for structural analysis. It is noteworthy that the Y-neighbor peaks are absent in both nanocrystal samples of Y_2O_3 and Y_2O_3:Tb. This can be explained by the fact that an increasing fraction of Y atoms are located near the nanoparticle surface as the particle size decreases. For these Y atoms, the location of neighboring atomic shells at an interatomic distance greater than the nearest-neighbor oxygen shell could become highly disordered, thereby resulting in a diminished EXAFS signal. A similar interpretation can also be applied to Fig. 7 which shows the local structures around Tb atoms in bulk and nanocrystals of Y_2O_3:Tb. In the bulk, there are near-neighbor peaks due to oxygen and Y; on the other hand, the Y peak disappears in the nanocrystals as a result of loss of coordination of the Y atoms or increased disorder in the nanoparticles.

The structural parameters around Y atoms obtained from curve fitting the EXAFS results (Figs. 4 and 6) are shown in Table I. A comparison of the first (oxygen) peak in Fig. 6, between the bulk and nanocrystal Y_2O_3 samples, shows a slight shift of the peak to a higher interatomic distance in the nanocrystals which can be related to local structural distortion and disorder. The oxygen peak for the nanocrystals might actually arise from an unresolved composite peak consisting of two somewhat disordered oxygen near-neighbor shells (corresponding to oxygen shells at 2.27 and 2.33 Å in bulk Y_2O_3). The apparent larger oxygen coordination number (5.7) for the first peak is also consistent with the existence of a composite oxygen shell in the nanocrystals. This apparent change in local Y–O bond length and oxygen coordination, together with the disappearance of the Y-neighbor peak, could be attributed to the distortion of local structures as a result of reduced size in the nanocrystals. However, Tb doping in Y_2O_3 nanocrystals does result in an increased coordination number of the nearest-neighbor oxygen shell (from 5.7 to 7.8) around the Y atoms (see Table I).

Table II presents the structural parameters around Tb atoms obtained from curve fitting the EXAFS results (Figs. 5 and 7). Bulk Y_2O_3:Tb has a larger nearest neighbor (Tb–O) distance (2.37 Å) than the nearest-neighbor (Y–O) distance in undoped bulk Y_2O_3 (2.27–2.33 Å). The second peak in Fig. 7 arises from two unresolved Y-neighbor shells around Tb, similar to those resolved Y-neighbor shells around Y in undoped bulk Y_2O_3 shown in Fig. 6. From a comparison of the local structures around Tb in bulk Y_2O_3:Tb with the similar local structures around Y in undoped bulk Y_2O_3 (see Tables I and II, Figs. 6 and 7), it can be concluded that Tb atoms can indeed substitute for Y sites in bulk Y_2O_3, while accompanied only by a slight local structural distortion around the dopant atoms.

For a comparison of the first (oxygen) peak around Tb between bulk and nanocrystals of Y_2O_3:Tb, it is clear that Tb doping in the nanocrystals results in not only a longer Tb–O bond length (2.42 Å), but also an increased oxygen coordination of 8.4 (see Table II). A comparison of the first peak around Y (Table I) and that around Tb (Table II) in the Tb-doped nanocrystals also shows that the local environment surrounding Tb suffers a significant distortion compared to the local structures around Y. The nanocrystals also show large disorder, indicated by the relatively higher values of the Debye–Waller factor σ^2 (a measure of local disorder) in these samples. It is conceivable that Tb doping in the nanocrystals is more complicated than in the bulk as a result of reduced particle size and higher degree of local disorder. In view of the results obtained thus far, we assert that Tb dopants in the nanocrystals of Y_2O_3 neither preferentially occupy the Y sites (as in the bulk material), nor can they all reside on Y sites deep in the center of the nanoparticles. The nanocrystals may have a rather distorted Y_2O_3 structure, and

Tb impurities can substitute somewhat randomly for Y sites in the small particles, probably with a significant fraction residing on the surface Y sites.

As a parenthetical remark, we have compared the present EXAFS results with our previous studies of Mn-doped nanocrystals of ZnS using Mn *K* edge EXAFS measurements.[9] The Mn activators were found to occupy mostly deep Zn sites well inside the ZnS:Mn nanocrystals, as manifested by the presence of the second and third neighboring shells in the Fourier transform. A capability to examine the location of impurity atoms is very useful for studying the DNC system. For device applications, in order to reduce the nonradiative energy dissipation near the surface of nanoparticles, it is important to prepare DNC phosphors with the activators located deep inside the nanoparticles. We have thus demonstrated that EXAFS is a unique tool well suited for this type of material characterization.

IV. CONCLUSION

Our x-ray excited luminescence data show pronounced changes and a significant difference between bulk and nanocrystal Y_2O_3:Tb at the Tb *L* edges, but only a moderate difference at the Y *K* edge. An energy transfer model is proposed to interpret these results. In connection with our EXAFS results, it is conceivable that a large fraction of Tb dopants occupy the sites near the nanoparticle surface of Y_2O_3:Tb, whereby the energy transfer from the irradiated Y_2O_3 host to the surface Tb atoms can be hindered due to nonradiative energy losses. The sharp jumps at the Tb *L* edges of the nanocrystals could be utilized for potential device applications.

Local structural changes in Y_2O_3 host material caused by reduced particle size and the effects of Tb doping in Y_2O_3:Tb nanocrystals have been studied by using the EXAFS technique. The effects of quantum confinement and chemical doping were examined around the Y *K* edge and Tb *L* edge on bulk and nanocrystal samples of Y_2O_3 and Y_2O_3:Tb. Our results show that chemical doping with dilute Tb in the bulk does not affect the average Y_2O_3 structure, while reducing particle size to nanometers can cause substantial changes in the material. The average Y–O bond length can increase and the Y sublattice may become highly disordered as a result of increased fraction of Y atoms residing on the surface sites in the nanocrystals. Tb doping can also increase the average coordination number of oxygen around Y atoms in the nanocrystals. The EXAFS data also indicate that local structure around Tb in bulk and nanocrystal Y_2O_3:Tb is similar to the local environment surrounding Y with some built-in local lattice distortion due to different ion sizes between Y and Tb. We conclude that Tb dopants substitute for Y sites in bulk Y_2O_3:Tb. The structures in nanocrystals of both Y_2O_3 and Y_2O_3:Tb can become more complicated due to the large fraction of surface atoms and higher degree of local disorder, although the EXAFS spectra around the Y *K* edge and Tb *L* edge appear similar. No Y–Y and Tb–Y peak can be discerned from the nearest-neighbor oxygen peak in the respective nanocrystals. This result is different from that of our previous study of Mn *K* edge EXAFS on ZnS:Mn nanocrystals in which most of Mn dopant atoms occupy deep Zn sites well inside the nanoparticles.

ACKNOWLEDGMENTS

The present research at SUNY-Buffalo is supported by U.S. Department of Energy under Grant No. DE-FG02-87ER45283. The SUNY X3 beamline at NSLS is supported by the Division of Basic Energy Sciences of the U.S. Department of Energy under Grant No. DE-FG02-86ER45231. Research carried out in part at the National Synchrotron Light Source is supported by the U.S. Department of Energy, Division of Materials Sciences and Division of Chemical Sciences.

[1] R. N. Bhargava, D. Gallagher, X. Hong, and A. Nurmikko, Phys. Rev. Lett. **72**, 416 (1994).
[2] R. N. Bhargava, J. Lumin. **70**, 85 (1996).
[3] E. T. Goldburt and R. N. Bhargava, J. Electrochem. Soc. Proc. **95–25**, 368 (1995).
[4] E. T. Goldburt, B. S. Kulkarni, R. N. Bhargava, J. Taylor, and M. Libera, Mater. Res. Soc. Symp. Proc. **424**, 441 (1997).
[5] This quantum confinement effect has caused a broadening in the photoluminescence excitation spectra of Y_2O_3:Tb nanocrystals, believed to be responsible for the ultrafast transfer of charge carriers from the host to the $^5D_3$ and $^5D_4$ states of the Tb^{3+} ions.
[6] R. Bhargava, J. Lumin. **72–74**, 46 (1997).
[7] R. Bhargava (unpublished).
[8] E. T. Goldburt, B. Kulkarni, R. N. Bhargava, J. Taylor, and M. Libera, J. Lumin. **72–74**, 190 (1997).
[9] Y. L. Soo, Z. H. Ming, S. W. Huang, Y. H. Kao, R. N. Bhargava, and D. Gallagher, Phys. Rev. B **50**, 7602 (1994).
[10] M. Newville, P. Livin, Y. Yacoby, J. J. Rehr, and E. A. Stern, Phys. Rev. B **47**, 14126 (1993).
[11] P. A. Lee, P. H. Citrin, P. Eisenberger, and B. M. Kincaid, Rev. Mod. Phys. **53**, 760 (1981).
[12] D. E. Sayers and B. A. Bunker, in *X-ray Absorption*, edited by D. C. Koningsberger and R. Prins (Wiley, New York, 1988), p. 211.
[13] J. J. Rehr, J. Mustre de Leon, S. I. Zabinsky, and R. C. Albers, J. Am. Chem. Soc. **113**, 5135 (1991).
[14] The quantum efficiency η was carefully measured with a standard procedure taking into account the effects of reflection, transmission, and absorption. The results on size dependence have been discussed in more detail in Refs. 2, 4, 8, and plots of η vs. *D* were shown. Similarities between the results obtained with Y_2O_3:Tb and ZnS:Mn nanocrystals suggest that the method used for determining the η-*D* relationship is insensitive to small variations in the synthesis procedure.
[15] R. N. Bhargava, D. Gallagher, and T. Welker, J. Lumin. **60**, 275 (1994).
[16] R. W. G. Wyckoff, *Crystal Structures* (Interscience, New York, 1960).